

Synergetic effect of pyrene-based fluorescent probe for trace nitroaniline sensing

Received 00th January 20xx,
Accepted 00th January 20xx

DOI: 10.1039/x0xx00000x

Shaoling Li,^a Wei Liu, Xinyi Song, CR,? Chuan-Zeng Wang,^{*b} Xing Feng,^{*a}

Nitroaniline is not only an important chemical intermediate, but also a toxic waste for human health. Thus, it is necessary to develop efficient, sensitive, and specific technologies and materials for detecting nitroaniline to address this issue. In this work, two 2-hydroxypyrene moieties have been connected via the oxygen centres using different alkyl groups (methyl or *n*-amyl) or 1,4-ethylbenzene as a bridge. The target pyrene-based compounds exhibit pyrene-like optical behaviour, and possess hypersensitivity toward *p*-nitroaniline compared to the *o*- and *m*-nitroaniline isomers. Moreover, the probe **3a** (containing the methyl bridge) exhibits a limit of detection (LOD) as low as 6.18×10^{-9} M for *p*-nitroaniline. Therefore, these compounds have application potential for the detection of trace amounts of nitroaniline isomers.

Introduction

Aniline and its derivatives are important chemical intermediates for the preparation of various commercial chemical products, such as agrochemicals, polymers, medicines, organic dyes etc.¹ However, the overuse of such aniline compounds and the uncontrolled disposal of aniline-containing waste materials can result in serious water contamination and environment pollution.^{2,3} Among them, although nitroaniline is a vital intermediate in chemical engineering,⁴ the intrinsic high toxicity toward the environment should not be ignored. Moreover, there is also a danger to human health, with diseases such as icterus jaundice, blood poisoning, skin eczema, and liver damage possible.^{5, 6} On the other hand, nitril-decorated nitroanilines display extremely high chemical stability, making them difficult to degrade, and so these types of compound can accumulate in living organisms via water, air and food chains.⁷ Thus, the development of highly efficient, sensitive and specific technologies/materials for the detection of nitroanilines is necessary.

Generally, traditional analytical technologies involving gas chromatography (GC), high performance liquid chromatography (HPLC) and related techniques, electrochemical analytical technologies and spectrophotometric methods have been widely applied in the

determination of nitroaniline compounds.⁸ Although these above-mentioned analytical technologies have some advantages such as fast response, low limit of detection (LOD) and considerable selectivity etc., their disadvantages, such as expensive equipment cost and poor portability, as well as complex experimental procedures have become apparent which has hampered their widespread use. Thus, fluorescent analytical methods are emerging as the cutting-edge technology for solving the problem, due to their convenient procedures, super-sensitivity, and fast response times.

For example, luminescent metal-organic frameworks (MOFs) not only can be an excellent fluorescent probes for selectively recognizing *p*-nitroaniline with a low detection limit,⁹⁻¹¹ but also display a high photocatalytic activity for the photodegradation of contaminates.^{4,12-13} Fluorescence dyes with white-light emission utilizing dicarboxylatopillar[5]arene (DCP5)-based coordination polymers have been reported to exhibit good detection performance toward nitroaromatic pollutants.¹⁴ Both the above-mentioned nitroaromatic detecting systems operate using a mechanism ascribed to photoinduced charge transfer (PCT), which results in a strong fluorescence quenching.

Pyrene^{15,16} is a typical four phenyl-fused polycyclic aromatic hydrocarbon compound, which displays intense blue fluorescence in solution ($\lambda_{em} = 372$ nm, $\Phi_f = 0.64$).¹⁷ However, pyrene prefers to form a dimer at high concentration, resulting in a red-shifted emission with fluorescence quenching.¹⁸ Due to its high luminescence efficiency, ease of chemical modification, and low cost, it is often used to design and synthesize fluorescent probe molecules. Based on the PCT mechanism, pyrene-based derivatives have served as fluorescent sensors for nitroaniline detection. Wang and co-workers synthesized 4,5,9,10-tetrasubstituted pyrenes^{19,20} and 1,3,6,8-tetrasubstituted pyrenes²¹ which exhibited a high sensitive

^a Guangdong Provincial Key Laboratory of Information Photonics Technology, School of Material and Energy, Guangdong University of Technology, Guangzhou, 510006, P. R. China Email: hyxhn@sina.com (X. Feng).

^b School of Chemistry and Chemical Engineering, Shandong University of Technology, Zibo 255049, P. R. China. E-mail: 13639028944@163.com (C.Z. Wang).

^c Beijing Institute of Graphic Communication, Beijing 102600, P.R. China. Hull? Electronic Supplementary Information (ESI) available: [details of any supplementary information available should be included here]. See DOI: 10.1039/x0xx00000x

response toward nitroaniline (NA) isomers with a low LOD. For example, the 4,5,9,10-functionalized tetrasubstituted pyrene show an especially specificity response towards *p*-nitroaniline with an LOD of $\sim 10^{-9}$ M, while the latter exhibits high sensitivity and selectivity for *o*-nitroaniline with LOD of $\sim 10^{-8}$ M. This maybe ascribed to the different molecular packing between the fluorescence probe with the nitroaniline isomers.²⁰

Generally, pyrene has 10 reactive sites, including the active sites (1-, 3-, 6- and 8-positions), the K-region (4-, 5-, 9- and 10-positions) and the nodal plane (2- and 7-positions), respectively. Among them, although substituents have been introduced at the 2- or 2,7-positions of pyrene, such systems display weak electronic communication, resulting in a “pyrene-like” photophysical properties behaviour. However, these substituents can play a significant role to affect the molecular packing via tuning the intramolecular interactions, and this can result in excellent emission behaviour.^{22,23} Herein, we have designed a set of pyrene-based molecules for nitroaniline detection, where two 2-hydroxypyrene units are connected by different alkyl (methyl or *n*-pentyl) or 1,4-ethylbenzene bridges;²⁴ the *n*-hexyl derivative was decorated at the 7-position to improve solubility. As expected, the three compounds display clear “pyrene-like” absorption, and the bridged unit exerts only a limited effect on the optical behaviour. On the other hand, the compound **3c** possesses a structure with higher rigidity that prefers to adopt π - π stacking, resulting in an excimer emission in the solid state. Moreover, due to the compounds containing two pyrene units, all compounds show a supra-sensitivity toward nitroaniline isomers, especially the *p*-nitroaniline which has the lowest LOD of $\sim 10^{-9}$ M. Thus, these compounds could be excellent fluorescence probes for trace nitroaniline sensing.

Results and discussion

Synthesis

The synthetic routes to the pyrene-based fluorescence probes **3a-c** are summarized in Scheme S1. The intermediate 2,7-dihydroxypyrene (**1**) was synthesized according to previous reports.^{22,25} An alkylation reaction of compound **1** with 1-iodohexane in a stoichiometric ratio of 1:1 afforded compounds **2**, which is further alkylated to afford the target compounds **3a-c** in considerable yield. Where the long *n*-hexyl chain was introduced at the 2-position, the solubility for both **2** and **3** was improved compared to the starting compound **1**. For example, compound **1** show considerable solubility in polar solvents, such as ethyl acetate or THF, but insoluble in non-polar solvents, while compounds **2** and **3** can dissolve in common solvents with good solubility. All intermediates and target compounds were fully characterized by ¹H/¹³C NMR spectroscopy and high-resolution mass spectrometry (HRMS).

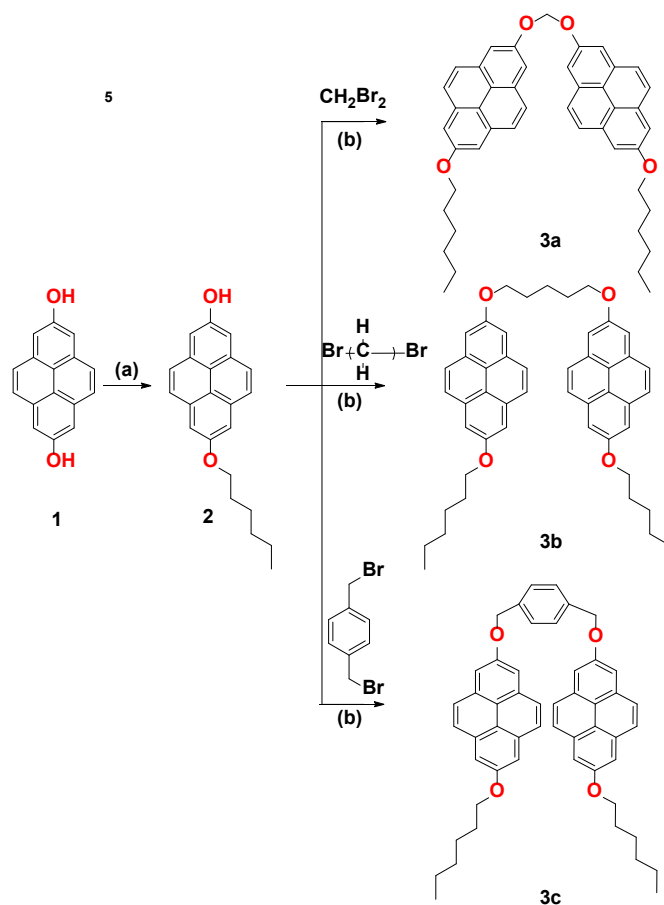


Figure 1. Synthetic route for pyrene-based compounds **3a-c**. (a) 1-iodohexane, Cs₂CO₃, DMF, (b) Cs₂CO₃, DMF.

Photophysical properties

The UV-vis absorption spectra and photoluminescence spectra of **3a-c** in dilute THF solution ($\sim 10^{-5}$ M) were studied at room temperature. The corresponding photophysical data are summarized in Table 1. As shown in Figure 2A, the UV-vis spectra of the three compounds exhibited similar absorption behaviour, with two different absorption bands in the range of 331-350 nm and 380-410 nm, respectively. The absorption band at the short-wavelength can be attributed to π - π^* transitions, while the absorption band at the long-wavelength originates from the characteristics of *n*- π^* transitions. Among the three compounds, the molar absorption coefficient (ϵ) of the short-wavelength absorption band increased from 68973 M⁻¹ cm⁻¹ (**3a**) to 82946 M⁻¹ cm⁻¹ (**3b**) and 76862 M⁻¹ cm⁻¹ (**3c**) as the chain length of the connecting group increased. The molar absorption coefficient (ϵ) of the long-wavelength absorption band increased from 7081 M⁻¹ cm⁻¹ (**3a**) to 10168 M⁻¹ cm⁻¹ (**3b**) and 9620 M⁻¹ cm⁻¹ (**3c**), indicating that the flexible degree could affect the ϵ , and the flexible molecule **3b** displays the largest ϵ in this case.

In THF solution, compounds **3a-c** exhibit dual emission, including the maximum emission peaks in range of 401-406 nm and shoulder emission peaks at 422-427 nm (Figure 2B). These compounds have similar fluorescence quantum yields (Φ_f) in solution in the order **3c** (0.41) > **3a** (0.35) > **3b** (0.33) (Figure 2D).

Compared with their solution behaviour, these compounds exhibit red-shifted emission (approximately 33-82 nm) with almost quenched fluorescence quantum yield in the solid state. Depending on the molecular conformation, the maximum red-shifted emission peak is at 442nm for **3a**, 488nm for **3b**, and 437nm for **3c**, respectively. This may be due to the presence of stronger intermolecular interactions caused by molecular aggregation in the solid state, resulting in a decrease in Φ_f in range 0.069-0.082 (Figure 2D).

Table 1. The photophysical properties of compounds **3a-c**

Compd	ε ($\lambda_{\max \text{ abs}}$) ($\text{M}^{-1} \text{ cm}^{-1}$)	$\lambda_{\max \text{ PL}}$	Φ_f	τ (ns)
		(nm) soln ^a /sol id ^b		
3a	340(68973) 395(7081)	401,422/ 442	0.35/0.069	10.35/4.71
3b	340(82946) 399(10168)	406,427 / 488	0.33/0.077	10.31/6.99
3c	340(76862) 399(9620)	404,426 / 437	0.41/0.082	11.49/1.19

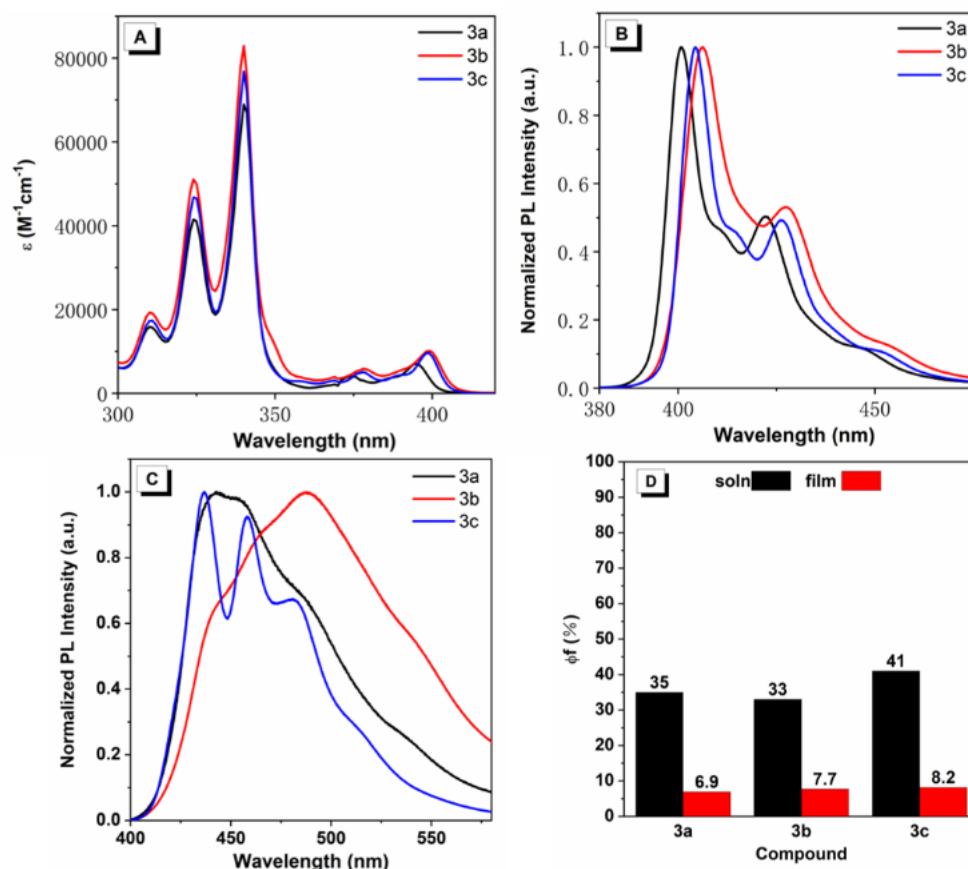


Figure 2. (A) UV-Vis spectra of compounds **3a-c**; (B) PL spectra of compounds **3a-c** in THF; (C) in the solid state at RT; (D) Quantum yields of compounds **3a-c** in solution (black) and solid state (red).

In addition, compounds **3a-c** show similar absorption behaviour in six different polar solvents, and the maximum absorption peak only shows a slight red-shift with the increase of solvent polarity, which indicates that the electronic structure of the compound in the ground state is independent of solvent polarity (Figures S12-S14). Similarly, compounds **3a-c** exhibit similar emissions in six different polar solvents. Taking compound **3a** as an example, as the solvent polarity increases from Cy to DMSO, the short wavelength emission exhibits a slight red-shifted emission from 400 nm to 403 nm, while the long wavelength emission exhibits a slight red-shifted emission from 420 nm to 423 nm, indicating that the solvation effect of this compound is not significant (Figure S12B). These results are

ascribed to the locally excited (LE) state rather than Intramolecular charge transfer.

The concentration dependent PL spectra of compound **3a-c** were determined. Taking compound **3a** as an example, within the concentration range of 10^{-7} - 10^{-5} M, compound **3a** has a maximum emission peak at 402 nm and a shoulder emission peak at 423 nm. As the concentration increases from 10^{-4} M to 10^{-3} M, the shoulder emission peak at 423 nm enhances, and there is a red-shifted attenuated emission peak at 413 nm (Figure S15). In addition, compounds **3b** and **3c** also exhibit similar concentration dependent PL behaviour (Figures S16-S17).

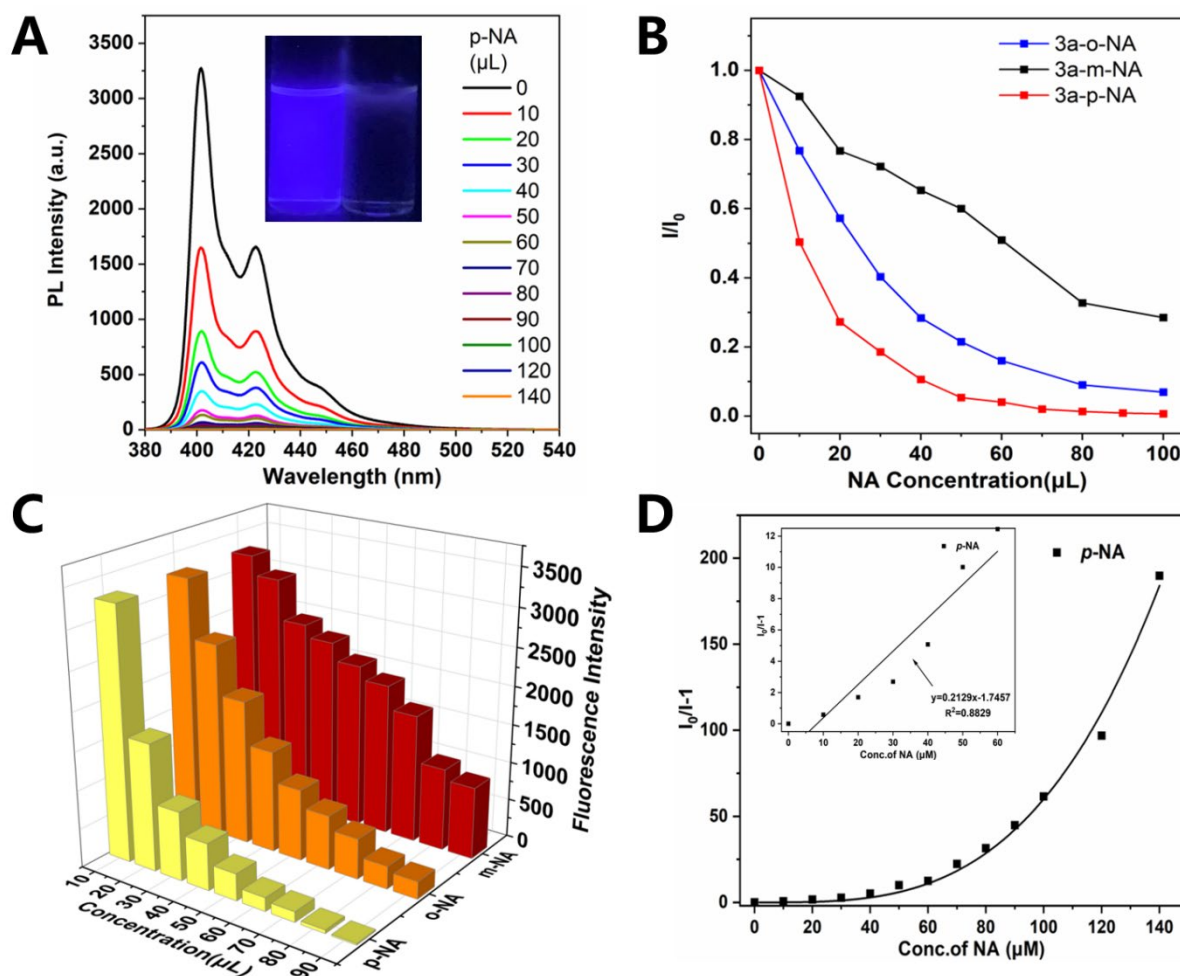


Figure 3. (A) Fluorescence quenching of **3a** with incremental addition of **p-NA** and inset photographs show the visible change in the fluorescence under UV light before and after addition of **p-NA**; (B) compound **3a** with NA relative PL intensity I/I_0 diagram; (C) histogram of fluorescence quenching of **3a** with NA; (D) Corresponding Stern-Volmer plots for quenching of **3a** with **p-NA** as quencher in DCM. Inset shows the Stern-Volmer plots at lower concentration of **p-NA**.

Previously, Wang *et al.* reported that pyrene derivatives could be chemosensor for nitroaromatic compounds detection with considerable sensitivity with a low limit of detection (LOD).^{19,20} Considering here that we have two pyrene units connected by an alkyl or aryl chain as a bridge, we infer that the compounds may exhibit a higher performance toward the sensing of the nitroaniline (NA) compounds with higher sensitivity and lower LOD. As shown in Figure 3A, the compound **3a** exhibits deep blue emission in THF solution, however, the emission intensity gradually decreased until completely quenched in the presence of the **o-NA**, **m-NA** or **p-NA** with a varied concentration from 0 to 100 μL , respectively. These results indicated that compound **3a** can detect the three NA isomer. The difference is that compound **3a** displays more sensitivity to **p-NA** even at super low concentration (Figures 3B-3C). The fluorescence is almost quenched, with a luminescence quenching efficiency of 99.3% for **p-NA**, 99.3% for 2-nitroaniline (**o-NA**) and 71.4% for 3-nitroaniline (**m-NA**) respectively, when the corresponding nitroaniline content reaches 100 μL . Compounds **3b** and **3c** also showed similar quenching efficiency, with **3b** having quenching rates of 92.2% for **o-NA**, 69% for **m-NA**, and 99.0% for **p-NA** (Figure S19); quenching rates for **3c** were **o-NA** 93.7%, **m-NA**

72.5%, and **p-NA** 99.5% (Figure S20). The LOD of the three pyrene-based emitters for nitroaniline detected by the Stern-Volmer (SV) equation: $(I_0/I) = 1 + K_{sv} [Q]$, where K_{sv} is the quenching constant (M^{-1}), $[Q]$ is the molar concentration of the nitro explosives ($m\text{M}$), I_0 and I are the fluorescence intensities before and after the addition of the nitro explosives, respectively. The results are summarized in Table S2. Although they have different molecular structures, the compounds herein exhibit a high affinity toward **p-NA** with a low LOD of $\sim 10^{-9}$ M.

DFT Calculations

To support our design strategy, the molecular optical and electronic properties of compounds **3a**, **3b**, and **3c** were studied. The geometric structure of the ground state of the molecule was optimized by density functional theory (DFT) calculations, reaching the B3LYP/6-31G (d, p) level. The energy levels of the highest occupied molecular orbital (HOMO) and the lowest unoccupied molecular orbital (LUMO) are shown in Figure 4. In the ground state, the HOMO and LUMO of compounds **3a**, **3b** and **3c** are mainly distributed on the pyrene ring, which is consistent with the insignificant solvation

discoloration effect, indicating that the intramolecular charge transfer behaviour is minimal in this symmetric system. This also indicates that there is no correlation between the intramolecular charge transfer and the length of the bridged alkyl chain. In addition, the energy gap between the

highest occupied molecular orbital (HOMO) and the lowest unoccupied molecular orbital of the three molecules is 3.76 eV. It can be inferred that compounds **3a-c** have the same maximum UV absorption wavelength, which is consistent with the above mentioned photophysical results.

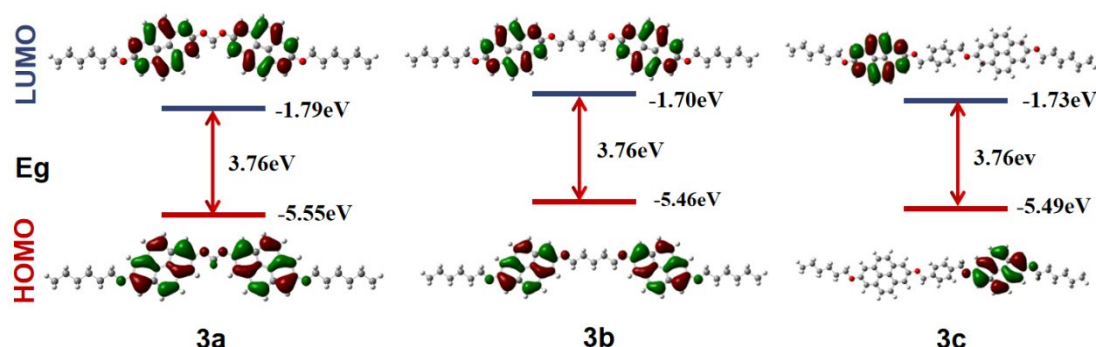


Figure 4. The electron density distribution and optimized ground state conformation of the HOMOs and LUMOs of **3a**, **3b** and **3c** based on density functional theory (DFT) at the B3LYP / 6-31G level.

Experimental

Synthetic procedures

Unless otherwise stated, all reagents used were purchased from commercial sources and were used without further purification. The starting compound pyrene-2,7-diol (**1**) was synthesized following the previously reported procedure.²²

Materials and methods

¹H and ¹³C NMR spectra were recorded on a Bruker AV 400M spectrometer using chloroform-*d* solvent and tetramethylsilane as internal reference. *J*-values are given in Hz. High-resolution mass spectra (HRMS) were recorded on a LC/MS/MS, which consisted of a HPLC system (Ultimate 3000 RSLC, Thermo Scientific, USA) and a Q Exactive Orbitrap (QE orbitrap type) mass spectrometer. UV-vis absorption spectra and photoluminescence (PL) spectra were recorded on a Shimadzu UV-2600 and the Hitachi F-4700 spectrofluorometer. PL quantum yields were measured using absolute methods using a Hamamatsu C11347-11 Quantaaurus-QY Analyzer. Thermogravimetric analysis was carried on a Mettler Toledo TGA/DSC3+ under dry nitrogen at a heating rate of 10 °C/min. The quantum chemistry calculation was performed on the Gaussian 09 (B3LYP/6-311G (d,p) basis set) software package.

Synthesis of 7-(hexyloxy)pyren-2-ol (**2**)

A mixture of **1** (530 mg, 2.26 mmol, 1 eq.), cesium carbonate (500 mg, 1.54 mmol, 0.67 eq.) and 1-iodohexane (382 mg, 1.8 mmol, 0.8 eq.) were added into dry *N,N*-dimethylformamide (8 mL). The reaction was refluxed for 24 h under nitrogen atmosphere. After cooling to room temperature, the mixture was quenched with water and extracted by dichloromethane (3 × 30 mL). The combined organic layer was washed with water and saturated brine (50 mL) and dried with anhydrous magnesium sulfate. The solvent was removed under reduced pressure, and the crude product was purified by column chromatography using a mixed eluent of CH₂Cl₂-hexane (1:3, v/v) to achieve a gray powder, which was further recrystallized

in a mixture solvent of CH₂Cl₂ and *n*-hexane (*V*_{DCM}: *V*_{hexane}=1:2) to obtain yellow crystals of sample **2** (200 mg, 70% yield). ¹H NMR (400 MHz, CDCl₃) δ 7.95 (d, *J* = 9.0 Hz, 2H), 7.91 (d, *J* = 9.0 Hz, 2H), 7.69 (s, 2H), 7.61 (s, 2H), 4.24 (t, *J* = 6.6 Hz, 2H), 2.02 – 1.75 (m, 2H), 1.57 (dd, *J* = 10.4, 4.7 Hz, 2H), 1.49 – 1.31 (m, 4H), 0.94 (t, *J* = 7.1 Hz, 3H) ppm.

Synthesis of bis((7-(hexyloxy)pyren-2-yl)oxy)methane (2Py-1C) (**3a**)

Following the general procedure, from the reaction of **2** (120 mg, 0.38 mmol, 2.2 eq.), cesium carbonate (500 mg, 1.54 mmol, 9 eq.) and diiodomethane (46 mg, 0.17 mmol, 1 eq.), **3a** was isolated in 73% yield (80 mg) as a white solid. ¹H NMR (400 MHz, CDCl₃) δ 8.11 – 7.86 (m, 12H), 7.70 (s, 4H), 6.24 (s, 2H), 4.25 (t, *J* = 6.6 Hz, 4H), 1.99 – 1.78 (m, 4H), 1.40 (dd, *J* = 7.2, 3.6 Hz, 8H), 0.93 (t, *J* = 7.0 Hz, 6H) ppm. ¹³C NMR (101 MHz, CDCl₃) δ 157.0, 154.5, 131.8, 131.6, 127.6, 127.5, 121.1, 119.9, 113.2, 111.4, 68.6, 53.4, 31.7, 29.5, 25.9, 22.7, 14.1 ppm. HRMS (ESI) *m/z*: [M + H]⁺ calcd for C₄₅H₄₄O₄, 649.33124; found, 649.33286.

Synthesis of 1,5-bis((7-(hexyloxy)pyren-2-yl)oxy)pentane (2Py-5C) (**3b**)

Following the general procedure, from the reaction of **2** (100 mg, 0.31 mmol, 2.2 eq.), cesium carbonate (500 mg, 1.54 mmol, 9 eq.) and 1,5-dibromopentane (32.8 mg, 0.14 mmol, 1 eq.), **3b** was isolated in 68% yield (68 mg) as a white solid. ¹H NMR (400 MHz, CDCl₃) δ 7.92 (d, *J* = 2.3 Hz, 8H), 7.68 (d, *J* = 4.1 Hz, 8H), 4.32 (t, *J* = 6.3 Hz, 4H), 4.24 (t, *J* = 6.6 Hz, 4H), 2.22 – 2.02 (m, 5H), 1.98 – 1.78 (m, 7H), 1.40 (dd, *J* = 7.2, 3.6 Hz, 9H), 0.94 (t, *J* = 7.0 Hz, 7H) ppm. ¹³C NMR (101 MHz, CDCl₃) δ 156.7, 156.6, 131.6, 127.4, 127.4, 120.1, 120.0, 111.3, 77.3, 77.0, 76.7, 68.6, 68.3, 53.4, 31.7, 29.5, 29.3, 25.9, 23.0, 22.7, 14.1 ppm. HRMS (ESI) *m/z*: [M + H]⁺ calcd for C₄₅H₅₂O₄, 705.39384; found, 705.39471.

Synthesis of 1,4-bis(((7-(hexyloxy)pyren-2-yl)oxy)methyl)benzene (2Py-Ph) (**3c**)

Following the general procedure, from the reaction of **2** (154 mg, 0.48 mmol, 2.2 eq.), cesium carbonate (500 mg, 1.54 mmol, 9 eq.) and 1,4-bis(bromomethyl)benzene (58 mg, 0.22 mmol, 1 eq.), **3c** was isolated in 61% yield (100 mg) as a light yellow solid. ¹H NMR (400 MHz, CDCl₃) δ 7.94 (s, 8H), 7.76 (s, 4H), 7.69 (s, 4H), 7.61 (s, 4H), 5.38 (s, 4H), 4.24 (t, *J* = 6.6 Hz, 4H), 2.05 – 1.87 (m, 4H), 1.40 (dd, *J* = 7.2, 3.6 Hz, 8H), 0.94 (t, *J* = 7.1 Hz, 6H) ppm. ¹³C NMR (101 MHz, CDCl₃) δ 156.8, 156.3, 137.0, 131.6, 131.6, 127.9, 127.6, 127.4, 120.3, 120.0, 111.6, 111.4, 70.3, 68.6, 53.4, 31.7, 31.6, 29.5, 25.9, 22.7, 14.1, 14.1 ppm. HRMS (ESI) *m/z*: [M + H]⁺ calcd for C₅₂H₅₀O₄, 739.37819; found, 739.38049.

Conclusions

In summary, this article presented a set of new pyrene-based fluorescent probes using different alkyl groups (methyl or *n*-amyl or 1,4-ethylbenzene) as bridges for connecting two hydroxypyrene derived moieties. Although both the 2,7-positions were substituted, these pyrene-based fluorescent probes still exhibit a “pyrene-like” absorption manner with deep blue emission in solution. However, due to molecular aggregation, these compounds exhibit various degrees of red-shifted emission, depending on the steric effect of the bridge units. Moreover, these compounds have been utilized as fluorescent sensors for the detection of trace amounts of nitroaniline (**NA**) and exhibit excellent selectivity and sensitivity towards nitroaniline isomers. In particular, all compounds **3a-c** exhibit high affinity towards ***p*-NA**, with a competitive LOD as low as 10⁻⁹ M. When the content of nitroaniline reaches 100 μL, the luminescence quenching efficiency of **3a-c** on ***p*-NA** is as high as 99%.

Author Contributions

Shaoling Li: Investigation, resources and visualization. Wei Liu: Investigation. Xinyi Song: Investigation. Chuan-Zeng Wang: Data curation and Writing - review & editing. Carl Redshaw: Writing - review & editing. Xing Feng: Data curation, conceptualization, Writing-original draft, supervision, project administration.

Conflicts of interest

There are no conflicts to declare.

Acknowledgements

This work was supported by the National Natural Science Foundation of China (21975054), Guangdong Provincial Key Laboratory of Information Photonics Technology (2020B121201011), the Open Fund of Guangdong Provincial Key Laboratory of Luminescence from Molecular Aggregates, Guangzhou 510640, China (South China University of Technology) (2019B030301003), Science and Technology Planning Project of Hunan Province (2018TP1017). CR thanks the University of Hull for support.

‡ Footnotes relating to the main text should appear here. These might include comments relevant not central to the matter under discussion, limited experimental and spectral data. 没有单晶?

§

§§

etc.

Notes and references

- 1 S. Morales-Torres, A. M. T. Silva, F. J. Maldonado-Hódar, B. F. Machado, A. F. Pérez-Cadenas, J. L. Faria, J. L. Figueiredo and F. Carrasco-Marín, *Appl. Catal., B: Environ.*, 2011, **105**, 86–94.
- 2 H. Ma, M. Wang, C. Pu, J. Zhang, S. Zhao, S. Yao and J. Xiong, *J. Hazard. Mater.*, 2009, **165**, 867–873.
- 3 T. Yang, C. Feng, P. Zhao, Y. Wu, Y. Ding, G. Wang and A. Hu, *J. Mater. Chem. C*, 2020, **8**, 2500–2506.
- 4 P. Wu, Y. Liu, Y. Li, M. Jiang, X. I. Li, Y. Shi and J. Wang, *J. Mater. Chem. A*, 2016, **4**, 16349–16355.
- 5 M. Chen, S. Xiang, P. Lv, C. Qi, H. T. Feng and B. Z. Tang, *Chem. Res. Chinese Universities*, 2021, **37**, 38–51.
- 6 M. N. Khatun, A. S. Tanwar, N. Meher and P. K. Iyer, *Chem. Eur. J.* 2016, **22**, 11898–11916.
- 7 J. Ghasemi and A. Niazi, *Talanta*, 2005, **65**, 1168–1173.
- 8 H. Wu and L. M. Du, *Spectrochim. Acta. A Mol. Biomol. Spectrosc.*, 2007, **67**, 976–979.
- 9 F. Wang, Z. Yu, C. Wang, K. Xu, J. Yu, J. Zhang, Y. Fu, X. Li and Y. Zhao, *Sens. Actuators B Chem.*, 2017, **239**, 688–695.
- 10 R. Zheng, Y. Zhang, G. Bao, P. Wu, W. Wei, X. Yuan, T. Zou, T. Zhang and J. Wang, *ACS Sustain. Chem. Eng.*, 2023, **11**, 9077–9086.
- 11 C. Ma, L. Zheng, G. Wang, J. Guo, L. Li, Q. He, Y. Chen and H. Zhang, *Aggregate.*, 2022, **3**: e145.
- 12 F. Wang, C. Wang, Z. Yu, Q. He, X. Li, C. Shang and Y. Zhao, *RSC Adv.*, 2015, **5**, 70086–70093.
- 13 C. Severi, S. Lahtinen, J. Rosenberg, A. Reisch, T. Soukka and A. S. Klymchenko, *Aggregate.*, 2022, **3**: e130.
- 14 X. S. Li, Y. F. Li, J. R. Wu, X. Y. Lou, J. Han, J. Qin and Y. W. Yang, *J. Mater. Chem. A*, 2020, **8**, 3651–3657.
- 15 X. Feng, J. Y. Hu, C. Redshaw and T. Yamato, *Chem. Eur. J.*, 2016, **22**, 11898 – 11916.
- 16 M. M. Islam, Z. Hu, Q. Wang, C. Redshaw and X. Feng, *Mater. Chem. Front.*, 2019, **3**, 762–781.
- 17 A. G. Crawford, A. D. Dwyer, Z. Liu, A. Steffen, A. Beeby, L. O. Pålsson, D. J. Tozer and T. B. Marder, *J. Am. Chem. Soc.*, 2011, **133**, 13349–13362.
- 18 Q. Peng and Z. Shuai, *Aggregate.* 2021, **2**: e91.
- 19 J. Y. Cao, Z. D. Yu, G. Yang, X. C. Wang, L. Jiang, X. Wang, W. X. Zhao, S. H. Chen, C. Redshaw, C.Z. Wang and T. Yamato, *J. Mol. Struct.*, 2023, **1285**, 135490.
- 20 H. L. Li, J. Y. Cao, Z. D. Yu, G. Yang, Z. M. Xue, C. Z. Wang, W. X. Zhao, Y. Zhao, C. Redshaw and T. Yamato, *Mater. Chem. Front.*, 2023, **7**, 3365–3372.
- 21 Z. D. Yu, J. Y. Cao, H. L. Li, G. Yang, W. X. Zhao, C. Z. Wang, S. H. Chen, M. R. J. Elsegood, C. Redshaw and T. Yamato, *J. Lumin.*, 2023, **253**, 119439.
- 22 X. Wang, J. Zhang, X. Mao, Y. Liu, R. Li, J. Bai, J. Zhang, C. Redshaw, X. Feng and B. Z. Tang, *J. Org. Chem.*, 2022, **87**, 8503–8514.
- 23 X. Wang, C. Zhang, J. Zeng, X. Mao, C. Redshaw, G. Niu, X. Yu and X. Feng, *J. Org. Chem.* 2022, **87**, 12741–12748.
- 24 F. Xiao, Y. Li, J. Li, D. Lei, G. Wang, T. Zhang, X. Hu and X. Dou, *Aggregate.* 2023, **4**: e260.
- 25 A. G. Crawford, Z. Liu, I. A. I. Mkhaliid, M. H. Thibault, N. Schwarz, G. Alcaraz, A. Steffen, J. C. Collings, A. S. Batsanov, J. A. K. Howard and T. B. Marder, *Chem. Eur. J.* 2012, **18**, 5022 – 5035.